Bull Volcanol (1991) 53:559-570

Bulletin of Volcanology

© Springer-Verlag 1991

Particle fallout, thermal disequilibrium and volcanic plumes

Andrew W Woods[1]* **and Marcus I Bursik**[2]

[1] Institute of Geophysics and Planetary Physics, A-025, Scripps Institution of Oceanography, UCSD, La Jolla, CA 92093, USA
[2] Earth and Space Sciences Division, MS 183-501, Jet Propulsion Laboratory, California Institute of Technology, Pasadena, CA 91109, USA

Received January 25/Accepted March 11, 1991

Abstract. We develop a model of a volcanic eruption column that includes the effects of fallout of pyroclasts and thermal disequilibrium. We show that clast fallout, with no thermal disequilibrium, has only a small effect upon the column. However, disequilibrium changes column behaviour significantly, and can even induce collapse. Our results may explain the lower plume heights and less widely dispersed fallout of cone-forming eruptions contrasted with sheet-forming eruptions. The model also predicts that the transition from the gas thrust to the convective region in a column results in an inflection in dispersal curves, that some features of the stratigraphy common to many fall deposits may result from column velocity structure, and that there may exist a region near the volcanic vent in which maximum pyroclast size does not decrease significantly with distance.

Introduction

There has been significant interest in understanding the effects of the total grain-size distribution (Sparks et al. 1981) or initial population (Walker 1971) on the dynamics of and fallout from volcanic eruption columns (Suzuki 1973, 1983; Walker 1973, 1980, 1981a, 1981b; Self et al. 1974; Wilson et al. 1978; Murrow et al. 1980; Carey and Sigurdsson 1982; Hayakawa 1985). Recent advances in the modelling of eruption columns (Wilson and Walker 1987; Woods 1988) provide the theoretical background upon which we can build in order to investigate a variety of the effects of the total grain-size distribution on column and pyroclast behaviour.

Carey and Sparks (1986) and Wilson and Walker (1987) presented models to predict the height of fallout and the maximum ranges of different sized clasts elutriated from Plinian eruption columns. However, the effects of fallout were not fully incorporated into the subsequent motion of the material remaining in the column. In the present paper, we investigate the effects of fallout, and find that it becomes increasingly important as mean grain-size increases and clasts lose their thermal contact with plume gas. In addition, we examine the related problem of how the velocity structure of the column affects fallout below the laterally spreading umbrella cloud.

Model of particle fallout

Woods (1988) modelled the erupted material as a perfect gas, the properties of which were the mass-averaged properties of the constituent volcanic gas, pyroclasts and entrained atmosphere. Such an approximation is valid when the momentum and enthalpy exchanges are so rapid that the velocity and temperature are the same for all phases. This is essentially the case if all clasts are sufficiently small to remain in good thermal and dynamic contact with the gas. In the present work, however, we are interested in investigating the effects of different grain-size distributions on column dynamics. As a result, we allow clasts to fall out, and this may occur before significant amounts of heat or momentum have been transferred between phases. Hence, the perfect gas approximation is no longer necessarily valid. However, to maintain an important element of simplicity in our model, we assume that each clast moves at the gas velocity and that there is no momentum transfer between phases, i.e. gas and pyroclasts move in 'dynamic equilibrium.' When the clasts of a given size reach a height at which the drag force that the column would exert on equivalent stationary clasts equals the weight of the clasts, they fall out. We hypothesize that this approximation yields a valid representation of the maximum rise heights and fallout distances of submetre pyroclasts based on observations of plume structure and calculations of clast deceleration (see below and Appendix A). Fuller investigations of the dynamic interaction between the clasts and the co-

* Now at: Institute of Theoretical Geophysics, Department of Applied Mathematics and Theoretical Physics, Silver Street, Cambridge, CB3 9EW, UK

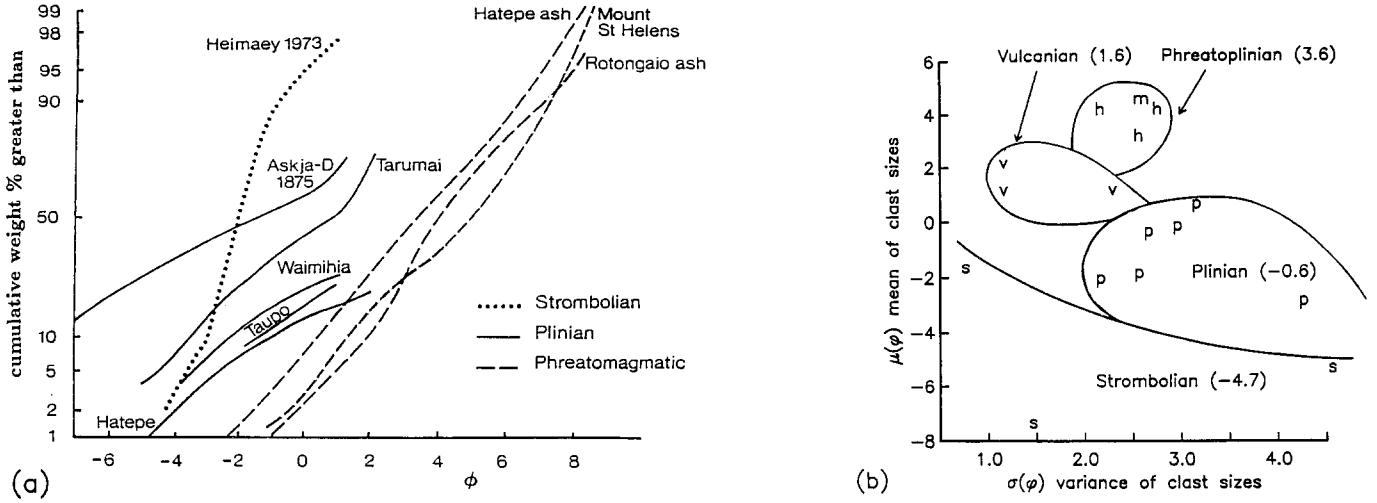

Fig. 1. **a** Cumulative grain-size distributions from several eruptions. **b** Plot of mean grain size versus the variance of the grain-size distribution for several eruptions; *m*, Mount St Helens, 18 May 1980, which may be phreatoplinian or coignimbrite (Carey and Sigurdsson 1982, Sparks et al. 1986). We have estimated μ_ϕ with the graphic mean and σ_ϕ with the inclusive graphic standard deviation of Folk (1979). Numbers in parentheses are average values of Md_ϕ for each class of eruption. See Table 1 for sources

Table 1. Total grain-size distributions of some fall deposits

Eruption	Type	$\mu_\phi \pm \sigma_\phi$	Reference
Askja C	Phreatoplinian	2.3±2.4	Sparks et al.1981
Hatepe ash	Phreatoplinian	3.3±2.3	Walker 1981a
Rotongaio ash	Phreatoplinian	4.0±1.9	Walker 1981a
Wairakei memb 3	Phreatoplinian	4.6±2.1	Self 1983
Hachinohe L	Phreatoplinian	4.2±2.5	Hayakawa 1985
Mount St Helens	Phreatoplinian (?) Coignimbrite (?)	4.4±2.3	Carey and Sigurdsson 1982
Cerro Negro 1968	Vulcanian	1.9±0.9	Rose et al. 1973
Cerro Negro 1971	Vulcanian	1.6±0.9	Rose et al. 1973
Fuego	Vulcanian	1.4±2.1	Morrow et al. 1980
Tarumai Ta	Plinian	0.4±2.7	Suzuki et al. 1973
Taupo	Plinian	0.3±2.7	Walker 1980; Pyle 1989
Askja D	Plinian	−2.6±4.1	Sparks et al. 1981
Waimihia	Plinian	−1.5±1.9	Walker 1981b; Pyle 1989
Hatepe	Plinian	1.1±3.0	Walker 1981b; Pyle 1989
Nambu	Plinian	−1.7±2.3	Hayakawa 1985
Chuseri	Plinian	−0.4±2.5	Hayakawa 1985
Stromboli	Strombolian	−6.8±1.3	Chouet et al. 1974
Heimaey	Strombolian	−2.1±0.6	Self et al. 1974
Etna, NE Crater	Strombolian	−5.2±4.4	McGetchin et al. 1974

lumn can be found in Bursik (1989), Carey et al. (1988) and Valentine and Wohletz (1989). In contrast to our assumption of dynamic equilibrium, we allow for some degree of 'thermal disequilibrium,' i.e. heat exchange between some clasts and the gas may not be instantaneous. In Appendix B, we show that only clasts smaller than ~3–4 mm (-2ϕ) in diameter are in thermal equilibrium with the gas. We therefore include a simple parameterisation of thermal equilibrium in order to model the most important thermal effects of the larger clasts.

In most, if not all, volcanic eruptions, nearly all pyroclasts have dimensions less than 24 cm ($> -8\phi$) and are therefore nearly in dynamic equilibrium with surrounding gas (Fig. 1; Table 1). However, those pyroclasts greater than $\sim -2\phi$ are not in thermal equilibrium (Table 2). Our parameterisation of thermal equilibrium allows us to explore some of the features of eruptions in which these larger clasts predominate. Thus, our work has certain ramifications for all eruption types, from Hawaiian to ultraplinian and phreato-

Table 2. Simple estimates of thermal disequilibrium, f (in equilibrium $f=1$)

Mean grain size (μ_ϕ)	f
$(\mu_\phi) > -2$	1.0
$-2 > (\mu_\phi) > -4$	0.9–1.0
$-4 > (\mu_\phi) > -5$	0.7–0.9
$-5 > (\mu_\phi) > -6$	0.3–0.7
$-6 > (\mu_\phi) > -7$	0.1–0.3
$-7 > (\mu_\phi)$	0.0–0.1

plinian. In drawing conclusions from our model, however, we exercise a considerable degree of caution, both because of the simplifications implicit in our parameterisation, but also because of our simple approximation of the complex nature of pyroclast fallout.

The total grain-size distribution

We represent the volume of clasts of diameter d, in mm, per unit volume of material in the column at height z by $P(d,z)$; we assume P has the form:

$$P(d,z)=p(d)\frac{A(0)u(0)}{A(z)u(z)} \text{ for } d<d(\max,z). \quad (1)$$

where $z=0$ refers to the origin, $p(d)$ gives the distribution of clast diameters, at the vent, which results from fragmentation processes in the conduit (Walker 1973), $A(z)$ and $u(z)$ are the cross-sectional area and velocity of the column and $d(\max,z)$ is the maximum clast size remaining in the column at height z. $p(d)$ is the total grain-size distribution. We have assumed that at any height the relative fraction of the different clast sizes which are still in the column is constant. All variables are defined in Table 3.

Field data (Fig. 1a) suggest that $p(d)$ follows a log-normal distribution given by:

$$p(d)=\frac{1}{\sqrt{2\pi}\,d\sigma_\phi}\exp\left(-\frac{(\log_2(d)-\mu_\phi)^2}{2\sigma_\phi^2}\right), \quad (2)$$

Table 3. List of variables and constants

A	cross sectional area of the column
C_d	drag coefficient
C_a	specific heat of air
C_m	specific heat of magmatic gas
C_s	specific heat of solids
d	clast diameter
d_m	diameter of largest clast
E	specific enthalpy of material in the column
f	thermal disequilibrium coefficient (1 = pure equilibrium, 0 = pure disequilibrium)
F_D	drag force on a clast
g	gravitational acceleration
k_c	entrainment constant
L	column radius
m_a	mass of air in column per unit height
m_m	mass of magmatic gas in column per unit height
m_s	mass of pyroclasts in column per unit height
m_s	mass flux of pyroclasts in column
n	gas mass fraction in column
P	fractional volume of clasts of diameter d in column
p	fractional volume of clasts of diameter d at vent
P_A	atmospheric pressure (see Woods 1988 for details)
R_g	bulk gas constant
u	velocity in column
u_e	entrainment velocity
z	height
α	ambient density
β	bulk density of column
θ	temperature of column
σ_ϕ	standard deviation of the grain-size distribution
μ_ϕ	mean grain-size

where μ_ϕ is the logarithmic (ϕ) mean and σ_ϕ is the standard deviation of the logarithms of the clast diameters, again in ϕ. In Fig. 1a, log-normal distributions plot as straight lines. Table 1 summarises the values of the mean and standard deviation of a number of fall deposits for which the total grain-size distribution has been calculated. These data are used to present an approximate categorisation of the styles of eruption depending upon the relationship between their mean and variance in Fig. 1b, in which we have assumed that the particle distribution follows Eq. 2.

If all clasts are assumed to have the same density ρ_s, then the total mass of particles m_s per unit height at a distance z above the vent, is given by:

$$m_s=\rho_s\frac{A(0)u(0)}{u(z)}\int_{0+}^{d_m}p(d)\,\mathrm{d}d. \quad (3)$$

The factor $A(0)u(0)/u(z)$ changes with height as parcels of fluid are stretched or compressed due to changes in the vertical velocity.

Fallout criterion

We assume that fallout occurs at the height at which the weight of the clast equals the upward drag force of the surrounding flow. Our assumption that all pyroclasts of a given size fall from one height is equivalent to assuming that all pyroclasts at a given locality in the deposit are of the same size ($\sigma_\phi\to 0$). This is a reasonable assumption given that the variance of the total grain-size distribution for fall deposits is generally greater than the variance at single localities (see Figure 8, McGetchin et al. 1974; Figure 2, Murrow et al. 1980; Figure 5, Walker 1980; and Fig. 1a, this study). We envisage that the fallout process is effected by turbulent eddies driving the particles to the edge of the column, at which point they fall into the ambient atmosphere. After the particles have fallen out, we assume that they have no further interaction with the column. In practice, they may affect the air subsequently entrained lower in the column or even be re-entrained. These effects are weak if most particles fall out high in the column at large radial distances from the column below. However, Carey et al. (1988) showed that in highly concentrated, particle-laden laboratory plumes, particle re-entrainment can contribute to partial collapse. In a volcanic plume, this effect may be partially offset by recycled clasts lowering the effective thermal disequilibrium because of their increased residence time.

To calculate the height at which clasts of a given size fall out, we use the expression for the drag force F_D:

$$F_D=\frac{\pi}{8}d^2C_D(\Delta u)^2\rho \quad (4)$$

where ρ is the density of the gas phase adjacent to the clasts in the column, C_D is the drag coefficient and Δu is the velocity of the clasts relative to the surrounding gas. Carey and Sparks (1986) estimated that $C_D\approx 0.75$ if d is taken as the average diameter of the clasts. Howev-

er, other workers have used a drag law based on the largest diameter of the clasts (Wilson and Walker 1987) with $C_D = 1.4$. When comparing model predictions with field data, the drag coefficient consistent with the method of data collection should be used. For simplicity we set $C_D = 1.0$. Equation 4 holds for clasts as small as 0.1 mm ($<3\phi$) in diameter (Suzuki 1973). In our model calculations, we used the bulk density of the column β for the density term ρ to evaluate the drag force. In practice, although the finer clasts do exert a drag on the large clasts (Saffman 1962), the effective density felt by the larger clasts is nevertheless smaller than the bulk density. However, this difference is probably negligible in most of an eruption column because the bulk column density is close to the density of the gas alone. Using β in Eq. 4 gives maximum fallout heights for the clasts. We deduce from (4) that a clast of maximum diameter d_m and density ρ_s ($\gg\beta$) will fall out of the column at the height z at which the velocity of the column $u(z)$ satisfies:

$$u^2(z) = \frac{4}{3}\left(\frac{d_m g \rho_s}{\beta C_D}\right) \tag{5}$$

where g is the acceleration due to gravity.

The largest clasts may be too massive to be carried by the column and instead will behave as ballistics (Wilson 1972). However, for intense eruptions, clasts need to be approximately of 20-cm-size dimensions $\sim -8\phi$ before their weight exceeds the drag force exerted by the surrounding column and they behave as ballistics (Appendix A). Hence a negligibly small fraction of the erupted clasts are large enough to behave as ballistics. We truncate $p(d)$ at 5 m, $\sim -12\phi$, since this seems to be about the dimension of the largest clasts found in fall deposits (Walker and Croasdale 1970; Self et al. 1980).

As in Woods (1988) we adopt a 'top-hat' profile for the column which assumes that at each height every physical property of the column takes one value in the column and a second value in the environment. Using the top-hat profile is mathematically equivalent to using a Gaussian profile with the same characteristic values for each physical property but a different effective radius (Morton et al. 1956). One simplification is that our model predicts a unique fallout height for each clast size, rather than a range of heights, as would occur with a Gaussian (or other) distribution.

By considering a control volume at a fixed height in the column (Woods 1988) we deduce that the total mass of clasts per unit height, m_s, changes with height according to the relation:

$$\frac{dm_s}{dz} = \frac{A(0)u(0)}{u(z)} p(d_m) \frac{d(d_m)}{dz} \rho_s - \frac{du}{dz}\frac{m_s}{u(z)}. \tag{6}$$

The mass flux of clasts; $\pi\dot{m}_s$, is given by

$$\dot{m}_s = \beta u L^2 (1-n), \tag{7}$$

where L is the column radius and n the gas mass fraction, changes with height according to:

$$\frac{d\dot{m}_s}{dz} = A(0)u(0)\,p(d_m)\frac{d(d_m)}{dz}\rho_s. \tag{8}$$

In the last two expressions, $d_m(z)$ is given by (5) and $d(d_m)/dz$ may be found by differentiating (5).

Model equations for the dynamics of the column

Following Woods (1988), the equation for the conservation of mass flux becomes:

$$\frac{d}{dz}(\beta u L^2) = 2u_e L\alpha + \frac{d\dot{m}_s}{dz} \tag{9}$$

where α is the ambient density and u_e the entrainment velocity. On the right-hand side, the first term represents the entrainment of the air and the second term the clast fallout. In this equation we need to specify the value of the entrainment velocity, u_e. In the basal gas thrust region, where $\alpha<\beta$, the column behaves as a dense jet, driven upwards by its inertia. Thus, an entrainment law may be derived from the jet model of Prandtl (1954); we use the relationship:

$$u_e = 0.09\left(\frac{\beta}{\alpha}\right)^{1/2} u \tag{10}$$

similar to Woods (1988). Higher in the column, in the convective region, where the entrained air has been heated sufficiently that $\alpha>\beta$, the column is driven upwards by its buoyancy (Sparks and Wilson 1976). In this region, we follow the work of Morton et al. (1956), who showed that the entrainment velocity is directly proportional to the vertical velocity:

$$u_e = k_c u, \tag{11}$$

where the entrainment constant $k_c \approx 0.09$ (Sparks 1986). The choice of (10) and (11) ensures that the entrainment velocity is continuous across the height at which $\beta=\alpha$.

The conservation of momentum flux is:

$$\frac{d}{dz}(\beta u^2 L^2) = g L^2(\alpha-\beta). \tag{12}$$

At height z in the column, the conservation of enthalpy flux becomes (Woods 1988)

$$\frac{d}{dz}(\beta u L^2 E) = 2u_e L\alpha\left(\frac{u_e^2}{2} + gz + E_e\right) + \frac{d\dot{m}_s}{dz}\left(E + gz + \frac{u^2}{2}\right) - \frac{d}{dz}\left(\beta u L^2\left(gz + \frac{u^2}{2}\right)\right) \tag{13}$$

where E is the specific enthalpy of the column material and E_e is the specific enthalpy of the ambient. The second term on the right-hand side of this equation represents the change of enthalpy due to the fallout. We assume that there is negligible phase change of water vapour to liquid water, which is a valid approximation for relatively dry eruptions in a dry atmosphere; however, such effects may be important in phreatomagmatic eruptions.

Since only the sub-centimetre-sized clasts remain in thermal equilibrium with the gases (Appendix B) we have introduced a disequilibrium coefficient f to represent the mass fraction of the clasts in thermal equilibrium with the gas (c.f. Wilson 1976). All other clasts are assumed to remain at the eruption temperature. This is a simple parameterisation that allows us to investigate the effect of disequilibrium. There is no formal derivation of f, and it can only model the qualitative effect of disequilibrium; however, as the mean grain-size increases, the mass fraction of clasts in thermal equilibrium with the gas decreases. In Table 2, we suggest a range of values for f as a function of mean grain-size estimated from Appendix B; we have attempted to include the uncertainty in the heat transfer coefficient in these estimates. f is introduced in the definition of the specific heat:

$$C_p = \frac{C_a m_a + f C_s m_s + C_m m_m}{m_a + m_m + m_s}, \tag{14}$$

where m denotes mass, the subscripts a, m and s denote entrained air, magmatic volatiles and solids, respectively and C the specific heat.

As in Woods (1988), the column density, β, is given by:

$$\frac{1}{\beta} = (1-n)\frac{1}{\rho_s} + \frac{nR_g\theta}{P_A}, \tag{15}$$

where n is the gas mass fraction in the column, θ the column temperature, ρ_s the (fixed) particle density and R_g is the gas constant for the column. P_A is assumed to equal the ambient pressure throughout the column (Woods 1988). In practice, the column pressure will only adjust to the atmospheric pressure once the flow in the column becomes subsonic, but this transition occurs in the basal, gas thrust region (Kieffer 1981; Kieffer and Sturtevant 1984; Valentine and Wohletz 1989) and so for most of the height of the column, this assumption is good. Strictly the model is only applicable above the small decompression region (≤ 1 km) above the vent. The definitions of the gas mass fraction, n, and gas constant, R_g, are given in Woods (1988). The system of equations outlined above forms a complete model for the dynamics of the column. The equations were integrated using a second-order Runge-Kutta algorithm to calculate the variations of the column properties with height and also the total column height. Each step in the integration was constrained to have a relative error less than 10^{-3}.

The role of fallout and disequilibrium on the column

In this section we describe the results of the numerical investigations of the column model. We use the model to extend the range of eruption conditions over which valid first-order predictions of column-rise height can be made. Furthermore, we argue here that the model provides valid approximations for the maximum rise heights and fallout ranges of pyroclasts falling from the gas thrust and convective regions. Although the time averaged velocity and particle concentration profiles in plumes are Gaussian in shape (Popper et al. 1974; Carey et al. 1988), instantaneous profiles show large variations in amplitude, and peak velocities and concentrations at plume margins are similar to those on the centreline. Papantoniou and List (1989) have shown that passive tracers injected into plumes are transported primarily in coherent structures (ring vortices) whose width is roughly equal to plume width and whose convection velocity is the same as the time mean central plume velocity. The Gaussian profile is, in fact, the result of the passage of the ring vortices and of the intervening, relatively quiescent ambient fluid, which is necessarily more concentrated toward the plume margins. Thus, our model assumption that particles are transported to their maximum height, where they are carried outward to the plume margin and then fall, is entirely consistent with their being carried within, then flung from the ring vortices when the average vortex convection velocity reaches their terminal fall velocity. The present model can thus be used to predict variations of maximum clast size with distance from vent for clasts falling from the convective and gas thrust regions.

In Fig. 2, we show heights of model columns as a function of initial μ_ϕ for various values of f; in this figure $\sigma_\phi = 1.0$ (solid) and 3.0 (dotted). As may be seen the results are relatively insensitive to variations in σ_ϕ within the range of volcanic interest. Two important results may be deduced from this figure. First, for a given value of disequilibrium, the column height is relatively insensitive to the mean grain size unless $\mu_\phi < -6$. The small increase in column height with mean grain size at these smaller values of μ_ϕ may be understood from Fig. 3. For reasonable values of μ_ϕ, virtually all clasts can be carried into the umbrella cloud. However, the mass of clasts remaining in the cloud at any height decreases as μ_ϕ decreases, causing the cloud to be less dense and rise higher. Second, thermal disequilibrium plays a crucial role in determining column height. As the amount of disequilibrium increases (smaller f), column height de-

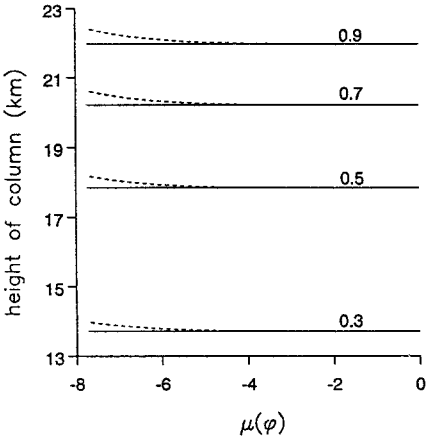

Fig. 2. Variation of column height with mean grain size for several values of the thermal disequilibrium parameter, f, which represents the mass fraction of the clasts in thermal equilibrium with the gas. $\sigma_\phi = 1.0$ (solid), $\sigma_\phi = 3.0$ (dotted)

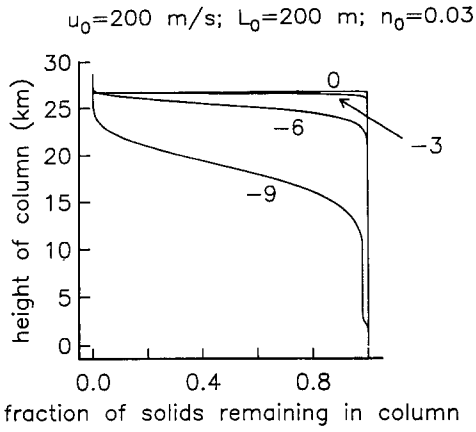

Fig. 3. Fraction of the clasts remaining in the column as a function of height for several mean grain sizes, shown in ϕ next to curves

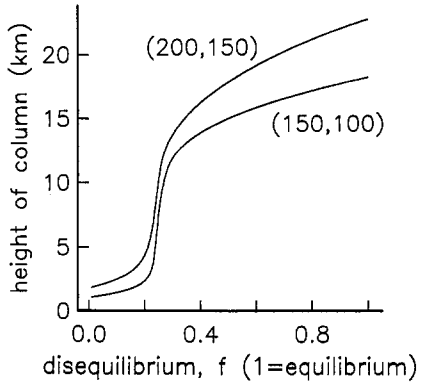

Fig. 4. Variation of the column height with the degree of disequilibrium, f, for two values of the eruption conditions at the vent (u_0, L_0)

creases significantly for a given μ_ϕ. This is because the thermal energy - hence buoyancy - available to drive the column upward decrease.

Figure 4 shows that, for two examples of eruption conditions, the column height decreases steadily with increasing disequilibrium until $f \approx 0.2$. At this point column height decreases dramatically to very small values. This jump in behaviour represents the transition between columns that become buoyant and rise convectively high into the atmosphere and columns that remain dense and form relatively low, collapsing fountains. Therefore, two eruptions of the same power, but different values of f, may generate very different columns. If f lies below some critical value, there may be insufficient thermal energy available for the erupting material to become buoyant before its upward velocity falls to zero and the eruption generates a collapsed fountain rather than a convective column. For a given eruptive power, the transition from a high buoyant column to a low collapsed fountain corresponds to a particular degree of disequilibrium. In the calculations of Fig. 4, we have set μ_ϕ and σ_ϕ equal to 1.0; in practice, changes in f are linked to changes in μ_ϕ, but in Fig. 2 we showed that, with $f=1$, changes in column height due to changes in μ_ϕ (and hence the fallout heights of the clasts) are relatively small: therefore it is the increase in thermal disequilibrium which causes the transition from a convective column to a collapsing fountain. It may be seen from Fig. 4 and Table 2, that when $\mu_\phi < -5$, the effect of thermal disequilibrium will become important in preventing the development of a convecting column.

These results suggest that column collapse not only depends upon an increasing mass eruption rate or decreasing vent velocity (Wilson et al. 1980), but also depends upon the mean grain size of the erupted material and hence the degree of thermal disequilibrium. We quantify the role of disequilibrium in determining collapse in Fig. 5, in which we have modified the collapse figure of Bursik and Woods (1991) to include the effect of disequilibrium as well as mass eruption rate and vent velocity. As the disequilibrium increases for a given erupted mass flux, column collapse may be induced at higher vent velocities. Therefore, a large degree of disequilibrium can prevent an otherwise violent eruption from generating a high column. Again, in this figure we have set $\mu_\phi = 1$ and $\sigma_\phi = 1$, since the conditions for collapse are not strongly dependent upon the different heights of clast fallout implied by different values of μ_ϕ. Therefore, typical values of μ_ϕ corresponding to the different values of f used in Fig. 5 may be deduced from Table 2.

The relationship between disequilibrium and collapse is further elucidated in Fig. 6, in which column or fountain height is shown as a function of mass flux for several values of disequilibrium. In this figure the mass flux is changed by varying the vent velocity, u_0. As u_0 and hence mass eruption rate decrease (for example, as a result of decreasing volatile content; Wilson et al. 1980), there is a sharp transition between buoyant columns and collapsed fountains if $f > \sim 0.2$. However, for $f < \sim 0.2$, convective columns cannot develop, i.e. the entire range of eruption conditions shown on Fig. 5 lies in the collapse region. For higher values of f, each transition from collapse to buoyancy on Fig. 6 corre-

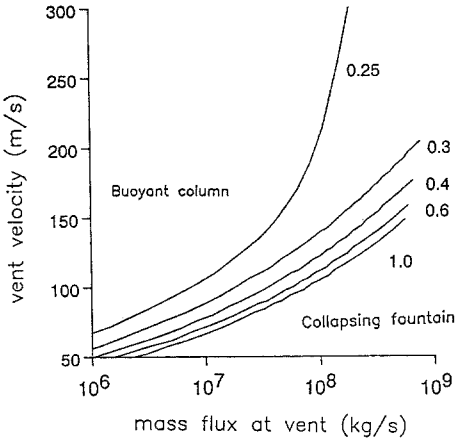

Fig. 5. Criteria for column collapse as a function of the velocity at the vent and the erupted mass flux for several values of the thermal disequilibrium f

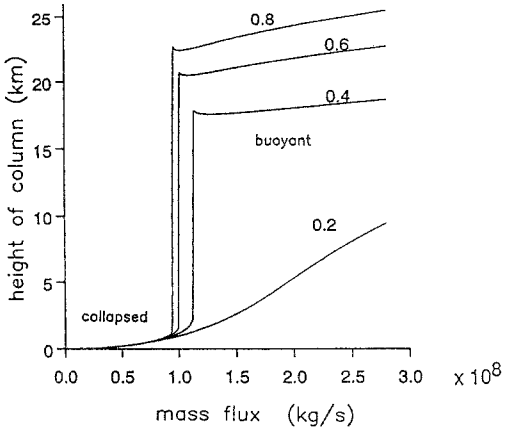

Fig. 6. Variation of column height with the erupted mass flux for a fixed vent radius as the initial velocity changes. The heights are shown for several values of the disequilibrium parameter, f.

sponds to one point on Fig. 5, and the trend in eruption conditions depicted in Fig. 6 would plot as curves oblique to both axes in Fig. 5.

The results presented in this section show that increasing disequilibrium enlarges the range of eruption conditions under which collapse occurs (Fig. 5). Furthermore, at some critical value of f, sufficient thermal energy to generate a convective column cannot become available, and realistic values of mass eruption rate and vent velocity result in a collapsing fountain. Table 2 shows that different values of μ_ϕ can be related, very approximately, to different values of f. We therefore infer that decreasing μ_ϕ (increasing grain size) not only changes the collapse criteria, but also that for each mass eruption rate and vent velocity there is a critical value of μ_ϕ below which a convective column cannot be generated. It may be seen from Table 2 and Fig. 5, that for $\mu_\phi < -6$ (approximately) the associated thermal disequilibrium between the clasts and the air is usually sufficient to inhibit generation of a convecting column.

Implications of disequilibrium induced collapse for fallout

The catastrophic drop in column height that occurs as f decreases, illustrated in Figs. 4 and 6, may have far-reaching implications for depositional patterns of the resulting pyroclastic units. Figure 6 suggests that even powerful eruptions with $f < \sim 0.2$ - those with coarse mean grain sizes (Table 2) - are incapable of generating convective columns. Most pyroclasts involved in such coarse-grained, fountaining eruptions will therefore fall out relatively near the vent to form a cinder or spatter cone. If, on the other hand, $f > \sim 0.2$, most pyroclasts can be carried high into a convective column and fall out in a widely dispersed sheet. These results suggest there is a fundamental difference in the processes responsible for cone-forming and sheet-forming eruptions (Walker 1973). The sharp decrease in dispersal distance that marks the transition between cone-forming and sheet-forming eruptions suggests that there is not a continuum in eruption behaviour between the two.

One further feature that differentiates some cone-forming eruptions from sheet-forming eruptions is that the former may also contain a significant proportion of pyroclasts that are not only in thermal disequilibrium but also in dynamic disequilibrium with the gas. This is especially true for Hawaiian and to a lesser extent for Strombolian eruptions, in which large mean clast size (Fig. 1) and low vent velocity (McGetchin et al. 1974; Chouet et al. 1974; Blackburn et al. 1976; Vergniolle and Jaupart 1986) together result in emission of ballistic pyroclasts in dynamic as well as thermal disequilibrium. We stress, however, that dynamic disequilibrium is not a necessary condition for the cone-forming eruption style.

The coarse-grained fountaining that results when grain size and hence degree of thermal disequilibrium are large is quite different from the fountaining associated with column collapse, which is caused by an increasing discharge rate or decreasing vent velocity (Sparks and Wilson 1976; Wilson et al. 1980). The fountains associated with column collapse contain a large fraction of fine-grained pyroclasts and tend to generate pyroclastic flows. There is a spectrum of fountaining behaviour between the coarse- and fine-grained fountain end-members. It is possible that a predominantly coarse-grained fountain falling on a steep slope might generate a pyroclastic flow, as occurred, for example, during the eruption of Mayon in 1968 (Moore and Melson 1969).

The effects of column velocity structure on fallout

Our model predicts that the range of different velocity structures associated with sheet-forming eruptions can produce distinct grain-size variations in the resulting deposits. We now examine the influence of the dynamic structure of the column on some features of the deposits generated by convective columns.

Variation of maximum clast size with distance from the vent

An inflexion in plots of the size of the largest lithic fragments with distance from the vent has been noted in a number of fall deposits including Fogo A and 1563 (Walker and Croasdale 1970), Terceira B, E and F (Self 1976), and Tarawera 1886 (Walker et al. 1984; Pyle 1989). These inflexions typically occur at distances of ≤ 5 km from the vent and clast diameters of approximately 10 cm. A model run showing such an inflexion is presented in Fig. 7. In the model, this inflection occurs at the transition between fallout from the gas thrust region and fallout from the convective region.

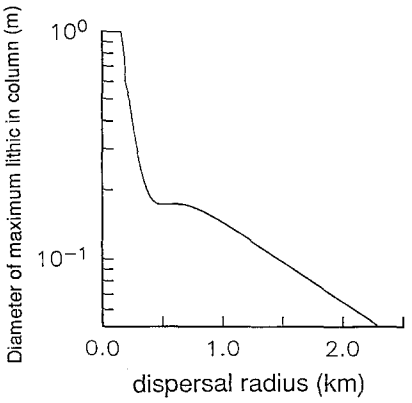

Fig. 7. Model lithic dispersal curve showing the inflection that is caused by the transition from the gas thrust to the convective region. The dispersal radius is calculated for the case of no wind or re-entrainment. For this run, $u_0 = 200$ m/s, $L_0 = 50$ m, and $n_0 = 0.03$ and the lithic density is taken as 2500 kg/m^3

This is because the rate of decrease of column velocity is much faster in the gas thrust region than in the convective region. Therefore, we hypothesize that the inflection in the data curves is also the result of this transition.

The role of superbuoyancy in producing reversed grading and stratification

One of the main predictions of the model of Woods (1988) was that the vertical velocity profile in the column does not necessarily decrease monotonically with height because of acceleration in the convective region. This effect has been explored further by Bursik and Woods (1991), who introduced the terminology 'superbuoyant' for a column whose velocity increases with height in the convective region. Superbuoyancy arises in model eruption columns with either low initial velocities or large vent radii. The resulting complex velocity structure may have important effects on fallout patterns. For example, if mass eruption rate increases while vent velocity remains fixed, as may happen during an episode of vent erosion (Wilson et al. 1980), then a column can evolve from being buoyant to superbuoyant. The increase in intensity initially results in greater ranges for the pyroclasts and therefore reversed grading (Sparks and Wilson 1976; Wilson et al. 1980). However, as the mass eruption rate increases further, column velocity falls to lower values before the erupted material becomes buoyant and the convective region develops (Fig. 8a). As a result, clasts within a certain size range will fall out closer to the vent (Fig. 8b) and parts of the deposit may tend toward normal or even complex stratification just before collapse occurs (Fig. 8c). This mechanism may therefore provide a partial explanation for the stratification and normal grading in the upper parts of proximal fall deposits underlying pyroclastic flows that resulted from collapse; such stratification has been recorded in the Vesuvius, A.D. 79 (Carey and Sigurdsson 1987) and Fogo A (Walker and Croasdale 1970) deposits.

A second depositional feature may result from superbuoyancy. In the gas thrust region, column velocity decreases rapidly and therefore maximum clast size decreases rapidly with distance from the vent, as discussed in the preceding subsection. However, once the column enters the convective region, the increasing velocity in the acceleration zone can result in sufficient support for the remaining clasts to be carried high into the convective region or even the umbrella cloud. As a result, there may be an area near the vent in which the maximum clast size does not significantly decrease with increasing distance (Fig. 9). This area corresponds to the acceleration region within the column. It may require dense sampling of a fall deposit to clearly discern this effect.

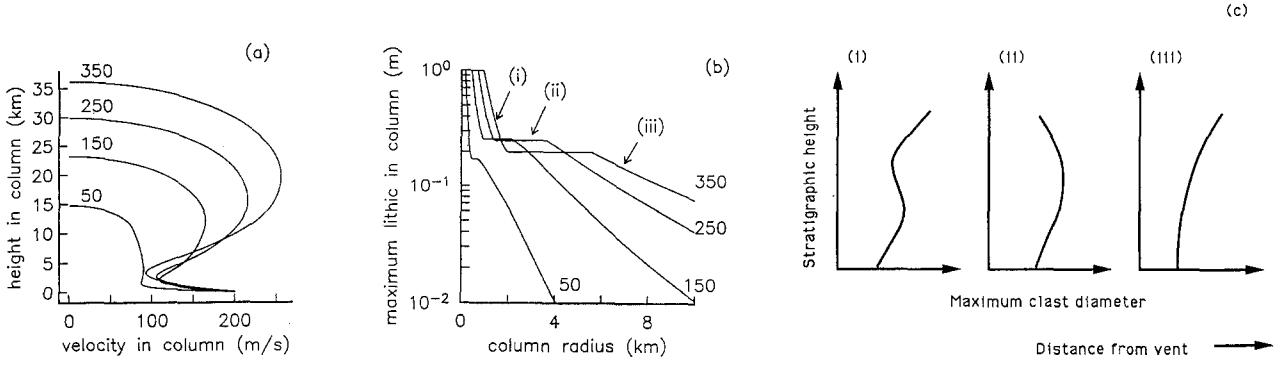

Fig. 8a–c. Illustration of the variation in (**a**) the column velocity with column height and (**b**) maximum lithic size with column radius as the vent radius changes from 50 m to 350 m (numbers on curves). **c** Schematic of the possible variation in maximum clast size with stratigraphic height at three locations from the vent ((*i*), (*ii*) and (*iii*) as marked on (b)) due to an increase in the vent radius prior to collapse (Carey and Sigurdsson 1989). Near the vent, (*i*), the acceleration zone can produce complex grading (cf. (b)). At intermediate distances, (*ii*), the grading becomes normal as the vent radius increases because the minimum velocity in the gas thrust region decreases (cf. (a)). At large distances, (*iii*), the deposit will remain reversely graded as long as the column has not collapsed

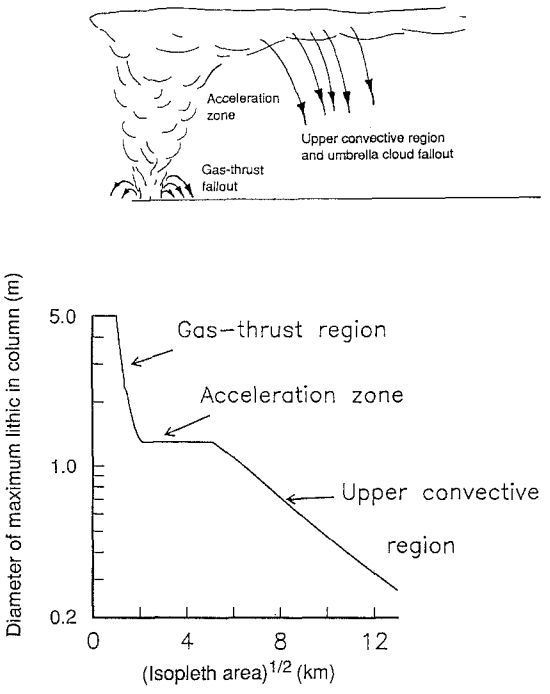

Fig. 9. **a** Schematic of the fallout from an eruption column. **b** Numerical calculation of the radius at which pumice clasts of different sizes and of density 500 kg/m^3 will fall out of the column, for a typical superbuoyant eruption in which $u_0 = 150$ m/s and $L_0 = 100$ m. The region in which the maximum clast size remains constant with radius corresponds to the acceleration zone

Discussion and conclusions

We have developed a self-consistent model for the fallout of particles from eruption columns and have investigated how fallout affects the dynamics of the column. We have included the important effects of thermal disequilibrium between the clasts and the gas. We have also examined the implications of this model for the proximal emplacement of pyroclasts. The main results of our work may be summarised as follows:

1. Thermal disequilibrium between the gas and clasts in an eruption column plays an important role in determining column height and dynamics, and subsequent dispersal of clasts. Increasing the mean grain size of the erupted material increases the degree of disequilibrium.
2. For the same mass eruption rate, column height decreases steadily as mean grain size and hence thermal disequilibrium increase, until a particular mean grain size is reached at which a convective column can no longer develop. Instead a relatively low, collapsed fountain, always denser than the surrounding atmosphere, is generated. Thermal disequilibrium therefore causes catastrophic changes in column behaviour.
3. The effects of particle fallout and loss of mass upon the dynamics and rise height of a column are slight unless coupled to the effects of thermal disequilibrium.
4. The generation of large eruption columns and the associated widespread dispersal of ash as tephra sheets require fine-grained pyroclasts in good thermal contact with gas. As a result of thermal disequilibrium, an eruption with a sufficiently coarse total grain-size distribution will produce a low fountain, leading to accumulation of coarse ejecta in cinder or spatter cones. Such coarse-grained fountains are mechanically different from the fine-grained fountains that develop when buoyant convecting columns collapse and that tend to produce pyroclastic flows.
5. Our model predicts that the transition from the gas thrust to the convective region in an eruption column is reflected in a sharp inflection in plots of maximum clast size versus distance from vent.
6. All columns must pass through a phase of superbuoyancy before they collapse. In the scenario of Sparks and Wilson (1976), mass flux increases preceding column collapse, tending to produce a reversely graded deposit. We have found that after the column becomes superbuoyant the minimum velocity in the gas thrust region eventually decreases, thus tending to produce complex grading in the fall deposits immediately underlying pyroclastic flows produced by column collapse. Superbuoyancy may explain the stratification found underneath collapse horizons.

Further developments of modelling fallout are numerous and we outline a number of possible extensions to this model below.

(a) A more realistic model of fallout (Armienti et al. 1989; Bursik et al. 1991) can be merged with the present column model, in order to determine how sedimentation of most pyroclasts, rather than just the largest, is linked with column dynamics.

(b) The effects of moisture may be incorporated into the model. Condensation of water vapour may be important to the column dynamics, especially in the formation of accretionary lapilli and in the phenomenon of rain-flushing. These water vapour effects may also influence the ability of a column to transport sulfate aerosols into the stratosphere (Self and Rampino 1988).

(c) The model could be used to estimate the amount of aerosol injectd into the upper atmosphere by eruptions with different total grain-size distributions and different degrees of thermal disequilibrium, possibly by synthesizing this model with Bursik's (1989) model of dynamic disequilibrium.

Acknowledgements. We thank Steve Sparks, Herbert Huppert, Grae Worster, Steve Self, Ken Wohletz, Mark Fahnestock and Steve Carey for helpful discussions and comments about this work. Steve Sparks and Steve Carey gave us some very penetrating and helpful reviews and we thank Steve Sparks for his encouragement. AWW would like to acknowledge St. John's College, Cambridge for a Research Fellowship and IGPP, SIO, UCSD for a Green Scholarship. MIB acknowledges the support of the North Atlantic Treaty Organisation via a grant awarded in 1988. The work was completed while MIB held a National Research Council-JPL (Caltech) Research Associateship.

Appendix A

We calculate the height over which clasts decelerate to zero vertical velocity from initially moving upwards with the column, at their terminal fall velocity. We show that for clasts smaller than 10 cm, this deceleration distance is very small compared to the height in the column at which the upward velocity of the column equals their terminal velocity. This calculation justifies our approximation that the particles instantly decelerate from moving with the column to coming to rest and falling out of the column.

We consider a particle, of speed v, moving in a column, of speed w, and assume that the clast decelerates under gravity from $v=w$ to $v=0$ according to the equation:

$$\frac{dv}{dt} = -g + \frac{3\beta}{4d\rho_s} C_d(v-w)^2 \tag{A1}$$

For simplicity, we assume that the height over which the particle decelerates is small compared to the height over which the column velocity, w, varies and so we take w as fixed over the region in which the clast decelerates (this assumption is self-consistent since the variation in column velocity, w, over the calculated height of deceleration is small). The clast will decelerate to zero vertical velocity if the column velocity w is such that the drag force it exerts on a stationary clast exactly balances the clast weight, giving:

$$g = \frac{3\beta}{4d\rho_s} C_d w^2 \tag{A2}$$

The clast can then hover in the column at this height until it falls out at the edge of the plume (assuming the 'top hat' profile). (A1) and (A2) give:

$$\int_w^v \frac{dv'}{(w^2-(w-v')^2)} = -\int_0^t \frac{g dt}{w^2} \tag{A3}$$

which may be readily integrated to give the clast velocity as a function of time:

$$v = 2w\left(1+\exp\left(\frac{2gt}{w}\right)\right)^{-1} \tag{A4}$$

The distance, H the clast travels vertically as it decelerates from moving with the column to coming to rest is therefore:

$$H = 2w\int_0^\infty \frac{dt}{\left(1+\exp\left(\frac{2gt}{w}\right)\right)} \tag{A5}$$

which reduces to:

$$H = \frac{w^2}{g}\log(2) \tag{A6}$$

Substituting the values for w and g into this equation, we obtain the result:

$$H = \frac{4\log(2)}{3}\frac{\rho_s}{\alpha}\frac{d}{C_d} \tag{A7}$$

which has the numerical value, using typical values for the parameters in the column:

$$H \sim 2500d \text{ m} \tag{A8}$$

where d is the particle diameter in metres. Thus a 20 cm clast decelerates over a height of the order of 500 m, while a 2 cm clast decelerates over a height of the order of 50 m. Over these height ranges, w does not change significantly, as may be seen in Figure 2 of Woods (1988) (except in the gas thrust region, where the velocity remains sufficiently large to support these clasts), and so our assumption that w is constant over the height through which the clast decelerates is valid.

For columns which ascend to heights ≥ 10 km, the approximate fallout model, outlined in the second section of this paper, is satisfactory for clasts which decelerate over heights ≤ 500 m. Hence we may apply the model to clasts ≤ 20 cm ($> -8\phi$), which includes both Plinian and Strombolian type eruptions (Fig. 1a).

Appendix B

We develop a simple model of heat transfer between pyroclasts and the gas phase that is more detailed than the one employed by Sparks and Wilson (1976). This model suggests that the assumption of thermal equilibrium is good for small clasts, which equilibrate very rapidly with the surrounding gas, but that for larger clasts there is a significant relaxation time over which the clasts adjust to thermal equilibrium with the gas. Before such a time has elapsed these particles may have fallen out of the column. Therefore an equilibrium model would overestimate the heat flux from clasts to the column, and therefore eruption column height as well.

As a simple model, we calculate how rapidly a spherical clast of diameter d cm cools due to the heat transfer between the clast and the gas which is rapidly flowing around it. We assume that the temperature of the gas in the column, T_g, is constant. In an eruption column, T_g decreases with height; however, by choosing a value of T_g between the maximum and minimum temperatures attained by the column, our calculation will yield an approximation for the time-scale required for cooling.

If we denote the surface temperature of the particle to be T_s then the rate of heat transfer from the particle to the gas is:

$$F_T = h_T(T_s - T_g) \tag{B1}$$

where h_T is an assumed heat transfer coefficient which parameterises both the convective and radiative cooling. The diffusion equation for the clast is:

$$\frac{\partial T}{\partial t} = \kappa\left(\frac{\partial^2 T}{\partial r^2} + \frac{2}{r}\frac{\partial T}{\partial r}\right) \tag{B2}$$

where κ is the thermal diffusivity and r is the radial coordinate. This equation may be solved analytically by noting that the quantity $u=rT$ satisfies the diffusion equation:

$$\frac{\partial u}{\partial t} = \kappa\frac{\partial^2 u}{\partial r^2}. \tag{B3}$$

We impose the boundary condition:

$$u(r=0)=0 \tag{B4}$$

since the centre of the particle has a finite temperature for all time. The solution of (B3) may be shown to be (Carslaw and Jaegar 1959, art 9.4):

$$T(r,t)\sim T_g+\frac{2h_T(T_0-T_g)}{\kappa r}\sum_{n=1}^{\infty}\exp(-\kappa\alpha_n^2 t)\left(\frac{\kappa^2 d^2\alpha_n^2+(dh_T-2\kappa)^2}{(\kappa^2 d^2\alpha_n^2+dh_T(dh_T-2\kappa))\alpha_n^2}\right)\sin(\alpha_n d/2)\sin(\alpha_n r) \tag{B5}$$

where α_n are roots of the equation:

$$\kappa d\alpha_n\cot(d\alpha_n/2)+dh_T-2\kappa=0. \tag{B6}$$

In the limit of rapid convective cooling, $h_T\gg\kappa/d$, and the smallest root of (B6), α_1, has the value $\alpha_1\sim 2\pi/d$. This suggests that the fraction of excess heat in the clast, after a long time τ is:

$$\frac{6}{\pi^2}\exp\left(\frac{-4\pi^2\kappa\tau}{d^2}\right) \tag{B7}$$

and so the time to equilibrate is:

$$\tau\sim 100d^2 s \tag{B8}$$

where we have assumed that the ratio of the heat transfer coefficient from the surface of the particle to the effective diffusive heat transfer coefficient within the particle satisfies $h_T d/2\kappa\gg 1$ and the diffusion coefficient $\kappa\approx 10^{-3}$. Since most columns rise to heights of the order of 10 km at velocities of about 100 m/s, a typical 'flight time' in the column is 100 s, and the largest particle that can equilibrate is of size $\sqrt{100/100}\approx 1.0$ cm or $\sim -3\phi$. We may assume thermal equilibrium between the column and clasts which equilibrate in a height less than about 1 km; the largest such clast has approximate size 0.3 – 0.4 cm (or $\phi\sim -2$). In the model outlined in the second section of the text we introduced a factor f to represent the fraction of the mass in thermal equilibrium with the solids. We have estimated f as a function of mean grain size in Table 2, based upon the excess heat content of the clasts in the lower 10 km of the column, according to (B5). This is only a simple parameterisation, but it allows us to identify the key features of disequilibrium, which thus become more important as the mean grain size increases.

References

Armienti P, Macedonio G, Pareschi MT (1989) A numerical model for simulation of tephra transport and deposition: applications to May 18 1890 Mount St Helens Eruption. J Geophys Res 93:6463-6476

Blackburn EA, Wilson L, Sparks RSJ (1976) Mechanisms and dynamics of strombolian activity. J Geol Soc Lond 132:429-440

Bursik M (1989) Effects of the drag force on the rise height of particles in the gas thrust region of volcanic eruption columns. Geophys Res Lett 16:441-444

Bursik MI, Sparks RSJ, Carey SN, Gilbert JS (1991) Dispersal of tephra by volcanic plumes: a study of the Fogo A eruption, Sao Miguel (Azores), subjudice, Bull Volcanol

Bursik MI, Woods AW (1991) Buoyant, superbuoyant and collapsing eruption columns. J Volcanol Geotherm Res 45, 347-350

Carey S, Sigurdsson H (1982) Influence of particle aggregation on deposition of distal tephra from from May 18 1980 eruption of Mount St Helens volcano. J Geophys Res 87:7061-7072

Carey S, Sigurdsson H (1987) Temporal variations in the column height and magma discharge rate during the AD 79 eruption of Vesuvius, Geol Soc Amer Bull 99:303-314

Carey S, Sigurdsson H, Sparks RSJ (1988) Experimental studies of particle laden plumes. J Geophys Res 93:15314-15328

Carey S, Sparks RSJ (1986) Quantitative models of the fall out and dispersal of tephra from volcanic eruption columns. Bull Volcanol 48:109-125

Carey S, Sigurdsson H (1989) The intensity of Plinian eruption columns. Bull Volcanol 51:28-40

Carslaw HS, Jaeger JC (1959) Conduction of heat in solids. Oxford University Press, Oxford, pp 1-510

Cas RAF, Wright JV (1987) Volcanic Successions. Allen and Unwin, London, pp 1-528

Chouet B, Hamisevisz N, McGetchin TR (1974) Photoballistics of volcanic jet activity at Stromboli, Italy. J Geophys Res 79:4961-4976

Folk RL (1979) Petrology of sedimentary rocks. Hemphill Press, Austin, Texas

Hayakawa Y (1985) Pyroclastic geology of Towada volcano. Bull Earthq Inst Univ Tokyo 60:507-592

Kieffer SW (1981) Fluid dynamics of the May 18 blast at Mount St Helens. USGS Prof Pap 1250:379-400

Kieffer S, Sturtevant B (1984) Laboratory studies of volcanic jets. J Geophys Res 89:8253-8268

McGetchin TR, Settle M, Chouet BA (1974) Cinder cone growth modeled after Northeast Crater, Mount Etna, Sicily. J Geophys Res 79:3257-3272

Moore JG, Melson WG (1969) Nuées ardentes of the 1968 eruption of Mayon Volcano, Philippines. Bull Volcanol 33:600-620

Morton B, Taylor Sir G, Turner S (1956) Turbulent gravitational convection from maintained and instantaneous sources. Proc R Soc A234:1-23

Murrow PJ, Rose WI, Self S (1980) Determination of the total grain size distribution in a vulcanian eruption column and its implications to stratospheric aerosol perturbation. Geophys Res Lett 7:893-895

Papantoniou D, List EJ (1989) Large-scale structure in the far field of buoyant jets. J Fluid Mech 209:151-190

Popper J, Abuaf N, Hetsroni G (1974) Velocity measurements in a two-phase turbulent jet. Int J Multiphase Flow 1:715-726

Prandtl LL (1954) Essential of fluid mechanics. Blackie, Glasgow

Pyle DI (1989) The thickness, volume and grain size of tephra fall deposits. Bull Volcanol 51:1-15

Rose WI, Bonis S, Stoiber RE, Keller M, Bickford T (1973) Studies of volcanic ash from two recent Central American eruptions. Bull Volcanol 37:338-364

Saffman P (1962) On the stability of laminar flow of a dusty gas. J Fluid Mech 13:120-128

Self S (1976) The Recent volcanology of Terceira, Azores. J geol Soc Lond 132:645-666

Self S (183) Large scale phreatomagmatic silicic volcanism: a case study from New Zealand. J Volcanol Geotherm Res 17:433-469

Self S, Kienle J, Huot J-P (1980) Ukinrek Maars, Alaska, II. Deposits and formation of the 1977 craters. J Volcanol Geotherm Res 7:39-65

Self S, Rampino MR (1988) The relationship between volcanic eruptions and climate change: still a conundrum? EOS 69:74-75, 85-86

Self S, Sparks RSJ, Booth B, Walker GPL (1974) The 1973 Heimay Strombolian scoria deposit, Iceland. Geol Mag 111:539–548

Sparks RSJ (1976) Grain-size variations in ignimbrites and implications for the transport of pyroclastic flows. Sedimentology 23:147–188

Sparks RSJ (1986) The dimensions and dynamics of volcanic eruption columns. Bull Volcanol 48:3–15

Sparks RSJ, Moore JG, Rice CJ (1986) The initial giant umbrella cloud of Mount St. Helens. J Volcanol Geotherm Res 28:257–274

Sparks RSJ, Wilson L (1976) A model for the formation of ignimbrite by gravitational collapse. J Geol Soc Lond 132:441–452

Sparks RSJ, Wilson L, Sigurdsson H (1981) The pyroclastic deposits of the 1875 eruption of Askja, Iceland. Philos Trans R Soc Lond A299:241–273

Suzuki T, Katsui Y, Nakamura T (1973) Size distribution of the Tarumai Ta-b pumicfall deposit. Bull Volcanol Soc Jap 18:47–64

Suzuki (1983) A theoretical model for the dispersion of tephra. In: Shimozuru D, Yokoyama I (eds) Arc volcanism: physics and tectonics. TERRAPUB, Toyko, pp 95–113

Valentine G, Wohletz KH (1989) Numerical models of Plinian eruption columns. J Geophys Res 94:1867–1887

Vergniolle S, Jaupart C (1986) Separated two-phase flow and basaltic eruptions. J Geophys Res 91:12842–12860

Walker GPL (1971) Grain-size characteristics of pyroclastic deposits, J Geology 79:696–714

Walker GPL (1973) Explosive volcanic eruptions – a new classification scheme. Geol Rundsch 62:431–446

Walker GPL (1980) The Taupo pumice: product of the most powerful known (ultraplinian) eruption? J Volcanol Geotherm Res 8:69–94

Walker GPL (1981a) Characteristics of two phreatoplinian ashes and their water-flushed origin. J Volcanol Geotherm Res 9:395–407

Walker GPL (1981b) The Waimihia and Hatepe plinian deposits from rhyolitic Taupo Volcanolic Centre. NZ J Geol Geophys 24:305–324

Walker GPL, Croasdale R (1970) Two plinian type eruptions in the Azores. J Geol Soc Lond 127:17–55

Walker GPL, Self S, Wilson L (1984) Tarawera, 1886, New Zealand – a basaltic plinian fissure eruption. J Volcanol Geotherm Res 21:61–78

Wilson L (1972) Explosive volcanic eruptions II – The atmospheric trajectories of pyroclasts. Geophys J R Astr Soc 30:381–392

Wilson L (1976) Explosive volcanic eruptions III – Plinian eruption columns. Geophys JR Astr Soc 45:543–556

Wilson L, Sparks RSJ, Huang TC, Watkins ND (1978) The control of eruption column heights by eruption energetics and dynamics. J Geophys Res 83:1829–1836

Wilson L, Sparks RSJ, Walker GPL (1980) Explosive volcanic eruptions IV – The control of magma properties and conduit geometry on eruption column behaviour. Geophys J R Astr Soc 63:117–148

Wilson L, Walker GPL (1987) Explosive volcanic eruptions IV – Ejecta dispersal in plinian eruptions: the control of eruption conditions and atmospheric properties. Geophys JR Astr Soc 89:651–679

Woods AW (1988) The fluid dynamics and thermodynamics of plinian eruption columns. Bull Volcanol 50:169–193

Editorial responsibility: R. S. J. Sparks